FERMILAB-CONF-14-563-ND

Status of NuMI experiments: MINOS+ and NOνA

João A. B. Coelho

Tufts University, Medford, Massachusetts 02155, USA
Email:joao.coelho@tufts.edu

The NuMI beam at Fermilab has been upgraded and is now capable of producing a 700 kW neutrino beam. Two major long-baseline neutrino experiments, MINOS+ and NOνA, have started data collection in the new NuMI configuration. This paper describes the latest developments of MINOS+ and NOνA. MINOS+ constitutes a new phase of the MINOS experiment and will provide improved sensitivity to new physics phenomena with a higher energy beam. NOνA will take advantage of its off-axis position to deliver precise measurements of $\nu_\mu \to \nu_e$ and $\bar{\nu}_\mu \to \bar{\nu}_e$ appearance, probing the neutrino mass ordering, the octant of θ_{23}, and the value of the CP violating phase δ_{CP}.

1 The NuMI Beam

The NuMI beam at Fermilab is the most powerful neutrino beam in operation, currently delivering 320 kW of beam power and capable of reaching 700 kW. It is host to two major long-baseline neutrino oscillation experiments: MINOS+ and NOνA. At the center of the beam, the MINOS+ detectors observe a broad energy spectrum that peaks at 7 GeV. The NOνA detectors are positioned 14 mrad off-axis yielding a narrow energy spectrum that peaks at 2 GeV, optimizing sensitivity to $\nu_\mu \to \nu_e$ transitions.

Since 2005, the NuMI beam has delivered more than 19.0×10^{20} Protons on Target (PoT), of which 3.3×10^{20} PoT were delivered in the new higher energy configuration for MINOS+ and NOνA.

2 MINOS+

The MINOS+ detectors are magnetized steel-scintillator tracking calorimeters. The near and far detectors are functionally identical and have a total mass of 0.98 kton and 5.4 kton respectively. The near detector is positioned at 1.04 km from the beam target and measures the neutrino flux and flavor composition at short distances while the far detectors is located 735 km from the beam target where oscillations due to the atmospheric mass splitting are expected to occur.

Neutrino interactions are classified based on their topologies, with ν_μ Charged Current (CC) interactions producing long muon tracks, while ν_e-CC and Neutral Current (NC) interactions form showers. The different profiles of electromagnetic and hadronic showers are used to distinguish ν_e-CC and NC interactions. A toroidal magnetic field enables both detectors to determine the muon charge to identify ν_μ and $\bar{\nu}_\mu$ CC interactions. Although ν_τ-CC interactions are very difficult to identify in the MINOS+ detectors, selections based on hadronic decays of the τ lepton are currently being developed. Tau neutrino appearance can also be inferred indirectly by comparing ν_μ-CC, ν_e-CC and NC interactions.

The latest results from MINOS+ combines all data taken in the low energy beam configuration from the MINOS era, including 14.07×10^{20} PoT of beam neutrino data and 37.87 kton-years of atmospheric neutrino data, separated into neutrinos and antineutrinos, and measuring ν_μ disappearance and ν_e appearance. An additional 10.8 kton-years of atmospheric neutrino data from the MINOS+ era has also been analyzed and the combined results yield the most precise measurement of the Δm^2_{32} parameter. The best fit values obtained are $\Delta m^2_{32} = 2.37^{+0.11}_{-0.07} \times 10^{-3}$ eV^2 for the inverted mass ordering and $\Delta m^2_{32} = 2.34^{+0.09}_{-0.09} \times 10^{-3}$ eV^2 for the normal mass ordering.

While the standard three-flavor picture of neutrino oscillations is able to explain the vast majority of the available neutrino data, a number of anomalies have been observed involving neutrinos in short-baselines. In particular, the LSND [2] and MiniBooNE [3] collaborations have observed significant excesses of ν_e-CC interactions in ν_μ beams consistent with oscillations occurring at $L/E \sim 1$ km/GeV. Such oscillations imply the existence of sterile neutrinos and would affect the rates of ν_μ-CC and NC interactions in MINOS.

Both the MINOS near and far detectors may be sensitive to active-sterile neutrino oscillations depending on the value of the additional mass splitting Δm^2_{43}. Three different regimes can be identified. Spectral distortions in the near detector are expected for $\Delta m^2_{43} \gg 0.5$ eV^2. If $\Delta m^2_{43} \sim 0.5$ eV^2, no oscillation occurs in the near detector and spectral distortions in the far detector are not observable, given its energy resolution, yielding a

Operated by Fermi Research Alliance, LLC under Contract No. De-AC02-07CH11359 with the United States Department of Energy.

relative rate measurement. Finally, for $\Delta m^2_{43} \ll 0.5$ eV^2, spectral distortions would be seen in the far detector, at high energies.

MINOS has performed a search for sterile neutrinos by measuring the ratios of far and near detector rates as a function of reconstructed neutrino energy. This search combines two separate samples of either ν_μ-CC interaction candidates or NC interaction candidates. No significant deviations from the standard three-flavor neutrino oscillation picture were found and this result imposes strong constraints on the 3+1 model of sterile neutrinos. Figure 1 shows the region of parameter space excluded by this MINOS analysis compared to results from previous experiments. A direct comparison with ν_e appearance results from LSND and MiniBooNE can be made by combining the ν_μ disappearance data from MINOS and the ν_e disappearance data from reactor experiments. Figure 2 shows an example of such combination where data from MINOS and Bugey are analyzed jointly to obtain limits on ν_e appearance at short baselines. This result excludes most of the parameter space favored by the LSND and MiniBooNE results, increasing the tension between disappearance and appearance experiments.

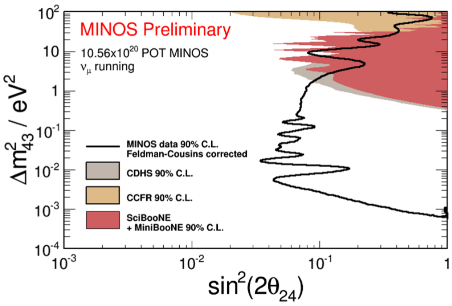

Figure 1: MINOS 90% confidence level contour on the sterile mixing parameters $\sin^2(2\theta_{24})$ and Δm^2_{43} compared with previous experiments. Regions of parameter space to the right of the contours are excluded at 90% CL.

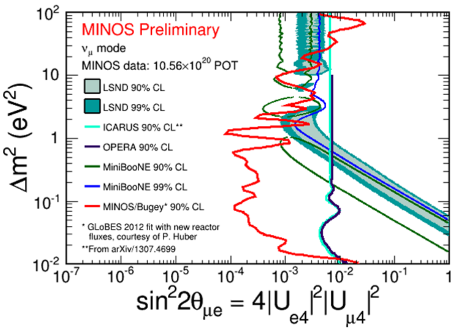

Figure 2: MINOS and Bugey combined 90% confidence level contour on the sterile mixing parameters $\sin^2(2\theta_{\mu e}) = 4|U_{e4}|^2|U_{\mu 4}|^2$ and Δm^2_{43}, obtained from the individual disappearance limits of each experiment on the size of $|U_{\mu 4}|^2$ and $|U_{e4}|^2$, respectively. Regions of parameter space to the right of the contour are excluded at 90% CL. The Bugey 90% CL limit is computed from a GLoBES 2012 fit provided by P. Huber. It accounts for the new calculation of reactor fluxes, as described in [4]. The MiniBooNE contours are those published in [3].

MINOS+ has already collected more than 3.3×10^{20} PoT. Figure 3 shows a preliminary comparison between the MINOS and MINOS+ data, indicating good agreement with the expected three-flavor oscillation prediction. These new data will substantially improve statistics in the 3-10 GeV neutrino energy range, enhancing the sensitivity to sterile neutrinos and other new physics phenomena.

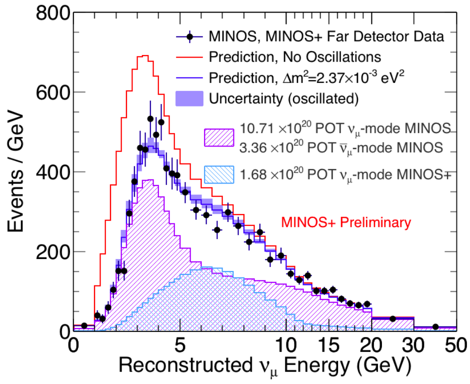

Figure 3: Selected ν_μ-CC candidates from MINOS and MINOS+ data as a function of reconstructed neutrino energy. The combined data sets show good agreement with the expected three-flavor oscillation prediction.

3 NOνA

The NOνA experiment represents the next generation of long-baseline neutrino experiments and is focused on measuring $\nu_\mu \to \nu_e$ appearance. NOνA takes advantage of an off-axis position with relation to the beam to tune the neutrino energy to a narrow window around the expected oscillation maximum, reducing the background from higher energy neutral current interactions.

The NOνA detectors [5] are highly active tracking calorimeters consisting of arrays of PVC cells filled with liquid scintillator. Each cell has cross-sectional dimensions of 4 cm $\times$ 6 cm and contains a wavelength-shifting fiber that collects the scintillation light and guides it to avalanche photo-diodes (APD) for readout. Near detector cells are 4.1 m long, while far detector cells are 15.6 m long. The detectors are built in alternating planes of horizontally and vertically aligned cells, rendering 3-D reconstruction of particle tracks. The segmentation of the NOνA detectors is much smaller than the 38 cm radiation length of the materials, dramatically improving identification of electromagnetic and hadronic showers with respect to the MINOS+ detectors.

Both near and far detectors have been completed and are taking data. The 0.3 kton near detector is positioned 105 m underground. The rate of neutrinos interactions in the near detector is much higher than the cosmic ray background and has been confirmed by measuring the activity in the detector synchronized with the beam pulses. The 14 kton far detector is a surface detector located 810 km from the beam target. The cosmic ray background in the far detector is many orders of magnitude larger than the neutrino signal, but timing, direction and containment information from reconstructed tracks have been successfully used to identify neutrino interactions from the NuMI beam.

NOνA will take data over the next 6 years and is expected to collect a total of 36×10^{20} PoT. Although designed to observe $\nu_\mu \to \nu_e$ appearance, NOνA will also be able to measure the ν_μ disappearance channel, determining $\sin^2(2\theta_{23})$ with 1% precision. In the first couple of years, NOνA will have sensitivity comparable to MINOS+ in the measurement of Δm^2_{32} and $\sin^2\theta_{23}$. The combined early sensitivity of MINOS+ and NOνA can be seen in Figure 4.

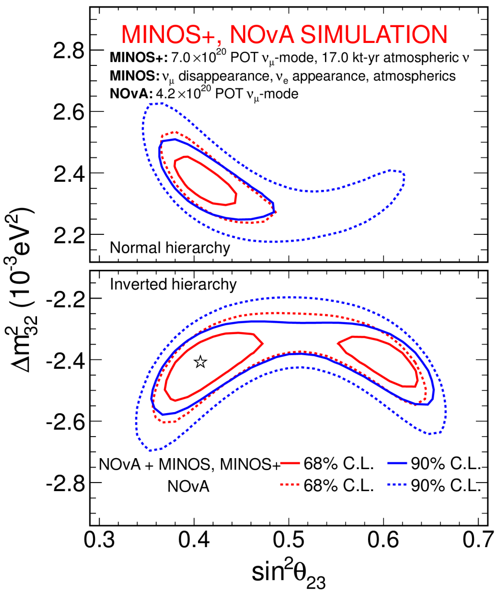

Figure 4: Combined early sensitivity of the MINOS+ and NOνA experiments to oscillation parameters Δm^2_{32} and $\sin^2\theta_{23}$.

Three quantities remain unknown in neutrino oscillation, namely the value of the CP violating phase δ_{CP}, the sign of the mass splitting Δm^2_{32}, and the octant of the mixing angle θ_{23}. All of these quantities are accessible through $\nu_\mu \to \nu_e$ appearance measurements. In particular, these quantities affect the relative rate of ν_e and $\bar{\nu}_e$ appearance in long-baseline experiments. Figure 5 shows an example of how NOνA will use neutrino and antineutrino measurements to determine these three remaining unknowns.

For comparison, Figure 6 shows the current knowledge of $\nu_\mu \to \nu_e$ and $\bar{\nu}_\mu \to \bar{\nu}_e$ appearance probabilities in the MINOS [6] and T2K [7] experiments and how they relate to these three unknown quantities. The MINOS data is compatible with all possible solutions in the three-flavor framework represented by the red and blue ellipses. The T2K data has already constrained some of the solutions, disfavoring the lower octant of θ_{23}, but a large fraction of the probability space remains unexplored.

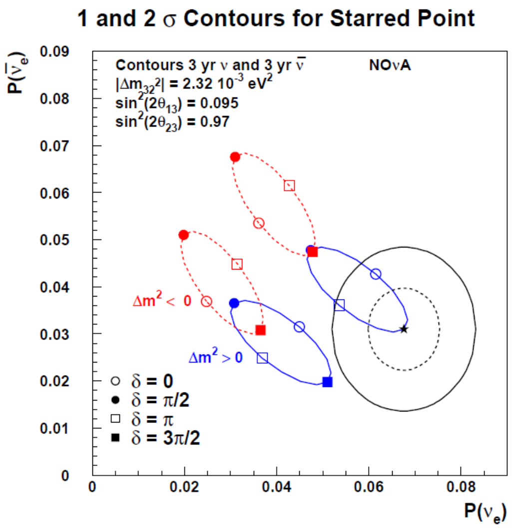

Figure 5: Probability of $\nu_\mu \to \nu_e$ and $\bar{\nu}_\mu \to \bar{\nu}_e$ appearance in NOνA at a neutrino energy of 2 GeV as a function of unknown quantities δ_{CP}, the octant of θ_{23} and the sign of Δm^2_{32}. The black lines represent an example of the expected sensitivity of NOνA to measuring the neutrino and antineutrino probabilities at 1σ (dashed line) and 2σ (solid line) confidence levels. The red and blue ellipses in the upper right (lower left) region represent probabilities for the upper (lower) octant of θ_{23}.

4 Summary

The MINOS experiments performed the most precise measurement of the Δm^2_{32} parameter within a three-flavor neutrino oscillation framework. These results combined data from the NuMI beam as well as atmospheric neutrinos and represent the first use of combined appearance and disappearance data by a long-baseline experiment. MINOS has also searched for active-sterile neutrino mixing by looking for addition spectral distortions in the ratio of far and near detector data. No evidence of oscillations was found, significantly disfavoring a sterile neutrino interpretation of the LSND and MiniBooNE ν_e excess. MINOS+ has already collected over 3.3×10^{20} PoT and will continue to test the three-flavor paradigm and to search for new phenomena in a broad range of energies.

The NOνA experiment has recently come online and is accumulating data towards a world-leading measurement of $\nu_\mu \to \nu_e$ appearance that will significantly improve our knowledge of the remaining unknown aspects of the three-flavor neutrino oscillation picture.

Acknowledgments

This work was supported by the U.S. DOE; the United Kingdom STFC; the U.S. NSF; the State and University of Minnesota; the University of Athens, Greece; Brazil's FAPESP, CNPq and CAPES.

References

[1] Adamson P *et al.* 2014 *Phys. Rev. Lett.* **112** 191801.

[2] Aguilar A *et al.* 2001 *Phys. Rev.* D **64** 112007.

[3] Aguilar-Arevalo A A *et al.* 2010, *Phys. Rev. Lett.* **105** 181801.

[4] Huber P 2011 *Phys. Rev.* C **85** 029901.

[5] D.S. Ayres *et al.* 2007, FERMILAB DESIGN-2007-01.

[6] Adamson P *et al.* 2013, *Phys. Rev. Lett.* **110** 171801

[7] K. Abe *et al.* 2014, *Phys. Rev. Lett.* **112** 061802.

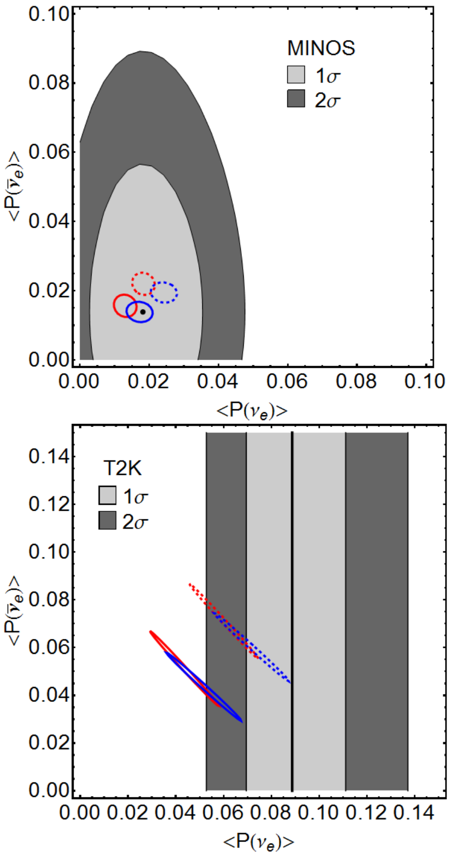

Figure 6: Average probability of $\nu_\mu \to \nu_e$ and $\bar{\nu}_\mu \to \bar{\nu}_e$ appearance in MINOS (top) and T2K (bottom) integrated over neutrino energy as a function of unknown quantities δ_{CP}, the octant of θ_{23} and the sign of Δm^2_{32}. The shaded contours represent the MINOS or T2K allowed regions at 1σ and 2σ confidence level. Blue and red lines represent probabilities for the normal and inverted mass orderings respectively at assorted values of δ_{CP}. Similarly, solid and dashed lines represent probabilities for the lower and upper octant of θ_{23} respectively.